

Impact of chaotic magnetic field on physical properties of rotating neutron stars

M. Lawrence Pattersons^{a,1}, Freddy P. Zen^{b,1,2}, Hadyan L. Prihadi^{c,3,2},
Muhammad F. A. R. Sakti^{d,4}, Getbogi Hikmawan^{e,1,2}

¹Theoretical High Energy Physics Group, Department of Physics, Institut Teknologi Bandung, Jl. Ganesha 10, Bandung 40132, Indonesia

²Indonesia Center for Theoretical and Mathematical Physics (ICTMP), Institut Teknologi Bandung, Jl. Ganesha 10, Bandung 40132, Indonesia

³Research Center for Quantum Physics, National Research and Innovation Agency (BRIN), South Tangerang 15314, Indonesia

⁴High Energy Physics Theory Group, Department of Physics, Faculty of Science, Chulalongkorn University, Bangkok 10330, Thailand

Abstract Observations reveal that magnetic fields on neutron stars (NSs) are in the range of 10^{8-15} G. Apart from being celestial bodies, NSs are normally rotating. In this work, we study the impact of a chaotic magnetic field on the physical properties of the rotating NSs. i.e. mass, radius, Kepler frequency, and moment of inertia. We employ an equation of state of NSs with the nuclei in the crust and hyperons in the core. Hartle-Thorne formalism as an approximation of the rotating NSs is utilized. For the magnetic field ansatz, we use the one coupled to the energy density. We find that the magnetic field can decrease radius of NS. NSs formed with higher central magnetic field strength and higher-order surface magnetic field strength exhibit a lower maximum mass compared to those formed with lower central magnetic field strength and lower-order surface magnetic field strength. In contrast, the increment of the magnetic field can increase the compactness and deformation of rotating NSs. As the magnetic field strength increases, the mass-radius curve begins to resemble that of quark stars. The presence of chaotic magnetic field enhances the Kepler frequency of rotating NSs, whereas it simultaneously tend to decreases their moment of inertia. The moment of inertia of rotating NSs with chaotic magnetic fields at $\Omega = 1000 \text{ s}^{-1}$ and $\Omega = 3000 \text{ s}^{-1}$ is consistent with the constraint range obtained from pulsar mass measurements, gravitational wave event data, and X-ray observations of emissions from hotspots on NS surfaces measured by NICER.

1 Introduction

It has been widely understood that the evolution of the massive stars whose mass is $8-25 M_{\odot}$ ends when neutron stars (NSs) form. The corresponding formation is due to the stars' gravitational collapse during Type-II, Ib, or Ic supernova explosion phenomena [1,2]. NSs are compact remnants of evolved stars, with degenerate fermions compressed by strong gravitational fields [3]. The stabilizing effect of gravity allows long-time-scale weak interactions (such as electron captures) to reach equilibrium, forming matter that is neutron-rich [4]. These stars cover an extensive density range, roughly several times of nuclear density ($n_0 \sim 10^{14} \text{ gm/cc}$), throughout their outer crust to their inner core [5]. NSs are normally rotating as all celestial objects tend to naturally always rotate due to the law of angular momentum conservation [6]. When rotating NSs are highly magnetized, they are recognized as pulsars [7,8,9,10].

NSs have a wide range of magnetic fields. Observations indicate that magnetic fields on NSs are at least in the range of 10^{8-15} G [3]. It is important to note that the direct observation of the magnetic field in NSs' cores remains unachieved. However, theoretical predictions suggest that the strengths of the magnetic fields in NSs' cores are in the order of 10^{18} G to 10^{20} G [11, 12,13]. New classes of pulsars such as Anomalous X-ray pulsars (AXPs) and Soft-Gamma Repeater pulsars (SGRs) have been identified producing vast magnetic fields. SGR is associated with remnants of a supernova, which is a young NS [14]. Highly magnetized NSs, i.e. magnetars, are typically slowly rotating NSs whose emission is thought to be powered by the decay of their large ($\geq 10^{12}$ G) magnetic fields, much greater than pulsars [15]. As well as their extreme magnetic fields,

^ae-mail: m.pattersons@proton.me

^be-mail: fpzen@fi.itb.ac.id

^ce-mail: hady001@brin.go.id

^de-mail: fitrahalfian@gmail.com

^ee-mail: getbogi@fi.itb.ac.id

magnetars are thought to have core temperature to be well above 10^9 K [16]. Moreover, observations on some AXPs also indicate that magnetic field of AXP's surface is around $10^{14} - 10^{15}$ G [14].

Konno et al. [17] calculated the deformation of NSs resulting from rotation and the presence of magnetic fields. In their analysis, a polytropic equation of state (EOS) was employed. Their findings indicate that for magnetars, the deformation induced by magnetic fields is dominant, whereas for typical pulsars, the magnetic effect is negligible. Mallick & Schramm [18] investigated mass corrections and the deformation of NSs under the influence of magnetic fields, treating the magnetic field as an anisotropy in the energy-momentum tensor (EMT). Interestingly, despite focusing on static NSs, their approach was based on the Hartle-Thorne (HT) formalism [19,20], which is typically applied to rotating relativistic stars. In their work, magnetic perturbations in static configurations were treated analogously to rotational perturbations, following the HT approximation. They considered both very stiff and very soft EOS models in their study. Lopes & Menezes [21] explored the effects of chaotic magnetic fields on NSs. A key advantage of incorporating a chaotic magnetic field lies in the elimination of anisotropy, simplifying the mathematical formulation. They also introduced an ansatz where the magnetic field is coupled to the energy density of the NS. For their EOS models, they utilized two variations: one including hyperons and one without hyperons. However, the rotation of NSs was not considered in their analysis.

On the other hand, in Newtonian theory, there exists a maximum rotational frequency for stars composed of perfect fluid, where gravitational and centrifugal forces are in equilibrium at their equators. This maximum frequency is proportional to the square root of the ratio of their masses to their radii [22]. In the context of general relativity (GR), the angular velocity of NSs is limited by the Kepler frequency, a threshold determined by their mass and radius in static configurations [23,24]. Notably, Refs. [22,23,24] provide specific calculations of the Kepler frequency.

Another significant property of NSs is their moment of inertia, which offers insights into their internal structure and EOS. Given the link between the EOS and moment of inertia, approximate methods for estimating it in static models, particularly for stiff EOS scenarios, are feasible [25]. Furthermore, measuring the moment of inertia is crucial due to its universal correlation with compactness [26]. Rahmansyah et al. [26] calculated the moment of inertia of anisotropic NS which satisfies the constraints proposed by Landry et al. [27]. However,

the magnetic field is not taken into account in their calculation of the moment of inertia.

Building on previous studies, we investigate the influence of the chaotic magnetic field on some physical properties of rotating NSs, i.e. mass, radius, Kepler frequency, and moment of inertia. The rotational aspects are modeled using the HT formalism, while the magnetic field is described by the Lopes-Menezes ansatz.

In general, NS has three parts with different compositions and density ranges i.e., outer crust, inner crust and the core [28]. The EOS employed in this work is based on the realistic model proposed by Miyatsu et al. [29], which includes nuclei in the crust and hyperons in the core. The algorithm of the numerical simulation follows the one used in Refs. [23,30].

The remainder of this paper is organized as follows. In Section 2, we outline the formulations employed in this study. Section 3 presents the numerical results and a discussion of their implications. Finally, we provide a summary of our findings in Section 4.

2 Mathematical Formulations

To make the discussion self-contained, in Sect. 2.1, we briefly review the chaotic magnetic field of NSs, while the HT formalism is given in Sect. 2.2. It is important to note that in the mathematical formulations we use $G = c = 1$.

2.1 Chaotic Magnetic Field of Neutron Stars

Generally, chaotically tangled magnetic field lines are thought to be present throughout astrophysical plasmas: planets, stars, accretion discs, galaxies, clusters of galaxies, and the intergalactic medium [31]. In nature, chaotic magnetic fields could be generated by asymmetric current configuration [32].

It has been widely understood that the magnetic field could generate anisotropy within NSs [11,14,18]. This problem would make the HT formalism for rotational configuration becomes more complex (please see Refs. [1,33,34]). For the magnetic field B in the z -direction, it is well-known that the stress tensor is written in the form: $diag(\frac{B^2}{8\pi}; \frac{B^2}{8\pi}; -\frac{B^2}{8\pi})$, being non identical [21]. In Ref. [35], it is argued that the effect of a magnetic field can be described using the concept of pressure only in the case of a small-scale chaotic field. Under this condition, the pressure due to the magnetic field p_B is shown to be consistent with field theory. Ref. [21] agreed to this argument. Now p_B reads

$$p_B = \frac{1}{3} \langle T_j^j \rangle = \frac{1}{3} \left(\frac{B^2}{8\pi} + \frac{B^2}{8\pi} - \frac{B^2}{8\pi} \right) = \frac{B^2}{24\pi}, \quad (1)$$

where T_j^j denotes the spatial components of the EMT. With this formulation in our hand, we can avoid the anisotropy which is caused by the appearance of magnetic field. The total energy density ϵ and total pressure p now write

$$\epsilon = \epsilon_m + \frac{B^2}{8\pi}, \quad (2)$$

$$p = p_m + \frac{B^2}{24\pi}, \quad (3)$$

where the subscript m stands for the matter contribution.

An ansatz of the magnetic field is proposed in Ref. [21], i.e.

$$B = B_0 \left(\frac{\epsilon_m}{\epsilon_0} \right)^\gamma + B_{surf}. \quad (4)$$

Here B_0 can be interpreted as the magnetic field at the center of the star, ϵ_0 is the energy density at the center of the NS with maximum mass when the magnetic field is zero, γ is any positive number (in this work we use $\gamma = 10^{-3}$)¹, and B_{surf} is the magnetic field at the surface of the NSs.

2.2 Hartle-Thorne Formalism for Rotating Relativistic Stars

The details of the HT formalism can be found in the original papers [19, 20]. Other interesting additional discussions on the formalism can be referred to Refs. [1, 30, 33, 34]. Here we present only a little discussion and the necessary equations to calculate some physical properties, i.e. mass, radius, Kepler frequency, and moment of inertia. This is especially useful to help the readers who are not familiar with the HT formalism.

It has to be noted that based on Eq. (2) and Eq. (3), it can be seen that the total energy density and total pressure arising from the matter and the presence of a magnetic field can be redefined by introducing ϵ and p . Therefore, in this subsection, the definitions of ϵ and p also encompass the total contributions from both matter and the magnetic field. Consequently, the formulation of HT presented in this subsection is indirectly modified by the presence of the magnetic field. Although this modification is not explicitly apparent, the contribution of the magnetic field is embedded within ϵ and p .

¹Values of γ around 10^{-3} yield similar results to the case of $\gamma = 10^{-3}$, while setting γ to much larger values (e.g., 1, 2, 3) significantly affects the outcome, likely due to changes in energy density affecting the core-crust transition.

In HT formalism, the metric reads [1, 19, 20, 30]

$$ds^2 = -e^{2\nu} dt^2 + e^{2\lambda} dr^2 + e^{2\psi} (d\phi - \omega dt)^2 + e^{2\mu} d\theta^2, \quad (5)$$

where ω is the angular velocity of the local inertial frame, which is proportional to the star's angular velocity Ω relative to a distant observer. In this case, ω and Ω satisfy $\omega = \Omega - \bar{\omega}$, where $\bar{\omega}$ is the angular velocity of the star relative to the local inertial frame.

Due to rotational perturbation, the exponential functions in Eq. (5) are expanded as the following:

$$e^{2\nu} = e^{2\varphi} [1 + 2(h_0 + h_2 P_2(\cos \theta))], \quad (6)$$

$$e^{2\lambda} = \left[1 + \frac{2}{r} (m_0 + m_2 P_2(\cos \theta)) \left(1 - \frac{2m(r)}{r} \right)^{-1} \right] \times \left(1 - \frac{2m(r)}{r} \right)^{-1} \quad (7)$$

$$e^{2\psi} = r^2 \sin^2 \theta [1 + 2(v_2 - h_2) P_2(\cos \theta)], \quad (8)$$

$$e^{2\mu} = r^2 [1 + 2(v_2 - h_2) P_2(\cos \theta)]. \quad (9)$$

Here h_0 , h_2 , m_0 , m_2 , and v_2 are functions of perturbation due to rotation; $P_2(\cos \theta)$ is the second order of Legendre polynomial; $e^{2\varphi}$ is a function which is constrained by

$$\frac{d\varphi}{dr} = \frac{m + 4\pi r^3 p}{r(r - 2m)}, \quad (10)$$

where m is the mass function which is constrained by

$$\frac{dm}{dr} = 4\pi r^2 \epsilon. \quad (11)$$

The equilibrium equation of the relativistic bodies is given by the Tolman-Oppenheimer-Volkoff (TOV) equation [1, 19, 36], i.e.

$$\frac{dp}{dr} = -(\epsilon + p) \frac{d\varphi}{dr}. \quad (12)$$

For a rotating configuration, $\bar{\omega}$ can be calculated by solving the following equation [19]:

$$\frac{1}{r^4} \frac{d}{dr} \left(r^4 j \frac{d\bar{\omega}}{dr} \right) + \frac{4}{r} \frac{dj}{dr} = 0, \quad (13)$$

where

$$j = e^{-\varphi} \left(1 - \frac{2m}{r} \right)^{1/2}. \quad (14)$$

The boundary condition at $r = 0$ is $\bar{\omega} = \omega_c$, where ω_c can be chosen arbitrarily.

It is important to note that Eqs. (10)–(12) deal with static configuration. Moreover, due to the rotation, the radius of the star is deformed. To obtain the mass and radius corrections of the rotating NS, we have to employ Einstein field equation

$$R_\nu^\mu - \frac{1}{2} \mathcal{R} \delta_\nu^\mu = 8\pi T_\nu^\mu, \quad (15)$$

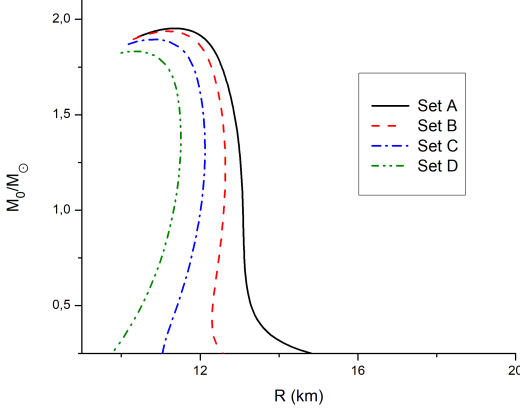


Fig. 1 Mass-radius relation of NSs for static configuration with different parameter sets of chaotic magnetic field strengths.

where R_{ν}^{μ} is Ricci tensor, \mathcal{R} is Ricci scalar, δ_{ν}^{μ} is Kronecker delta, and T_{ν}^{μ} denotes the EMT.

By calculating the Einstein field equation, for the (tt) component of the $l = 0$ order, we can obtain

$$\frac{dm_0}{dr} = 4\pi r^2 \frac{d\epsilon}{dp} (\epsilon + p) \mathcal{P}_0 + \frac{1}{12} j^2 r^4 \left(\frac{d\bar{\omega}}{dr} \right)^2 - \frac{1}{3} r^3 \left(\frac{dj^2}{dr} \right) \bar{\omega}^2. \quad (16)$$

From the (rr) component of the $l = 0$ order, we can obtain

$$\frac{d\mathcal{P}_0}{dr} = -\frac{m_0 (1 + 8\pi r^2 p)}{(r - 2m)^2} - \frac{8\pi r^2 (\epsilon + p)}{2(r - 2m)} \mathcal{P}_0 + \frac{1}{12} \times \frac{r^4 j^2}{r - 2m} \left(\frac{d\bar{\omega}}{dr} \right)^2 + \frac{1}{3} \left[\frac{d}{dr} \left(\frac{r^3 j^2 \bar{\omega}^2}{r - 2m} \right) \right]. \quad (17)$$

Here \mathcal{P}_0 is originally the 0th-order of expansion of pressure perturbation factor $\mathcal{P} = \mathcal{P}_0 + \mathcal{P}_2 P_2(\cos\theta)$. The boundary conditions at $r = 0$ are $m_0(0) = 0$ and $\mathcal{P}_0(0) = 0$.

Mass correction δM of the star is given by

$$\delta M = m_0(R) + \frac{L^2}{R^3}, \quad (18)$$

where R denotes the radius of the star, and L denotes the angular momentum, which satisfies

$$L = \frac{R^3}{2} (\Omega - \bar{\omega}(R)). \quad (19)$$

Thus, the total mass reads

$$M = M_0 + \delta M, \quad (20)$$

where M_0 is the mass of NSs within static configuration which is obtained by solving Eqs. (10)–(12) simultaneously.

From the $(\theta\theta)$, $(\phi\phi)$, (θr) , and (rr) components of the $l = 2$ order of Einstein field equation, we obtain

$$\frac{dv_2}{dr} = -2 \frac{d\varphi}{dr} h_2 + \left(\frac{1}{r} + \frac{d\varphi}{dr} \right) \times \left[-\frac{1}{3} r^3 \frac{dj^2}{dr} \bar{\omega}^2 + \frac{1}{6} j^2 r^4 \left(\frac{d\bar{\omega}}{dr} \right)^2 \right], \quad (21)$$

$$\begin{aligned} \frac{dh_2}{dr} = & -2 \frac{d\varphi}{dr} h_2 + \frac{[8\pi r(\epsilon + p) - \frac{4m}{r^2}]}{(r - 2m) \left(2 \frac{d\varphi}{dr} \right)} h_2 \\ & - \frac{4v_2}{r(r - 2m)} \left(2 \frac{d\varphi}{dr} \right)^{-1} + \frac{r^3 j^2}{6} \\ & \times \left[\frac{d\varphi}{dr} r - \frac{1}{(r - 2m) \left(2 \frac{d\varphi}{dr} \right)} \right] \left(\frac{d\bar{\omega}}{dr} \right)^2 \\ & - \frac{r^2 \bar{\omega}^2}{3} \left[\frac{d\varphi}{dr} + \frac{1}{(r - 2m) \left(2 \frac{d\varphi}{dr} \right)} \right] \frac{dj^2}{dr}. \end{aligned} \quad (22)$$

The boundary conditions at $r = 0$ are $v_2(0) = 0$ and $h_2 = 0$.

There exists a formula [1, 19]

$$\mathcal{P}_2 = -h_2 - \frac{1}{3} r^2 e^{-2\varphi} \bar{\omega}^2. \quad (23)$$

The radius correction of the star is given by

$$\delta r = \xi_0(R) + \xi_2(R) P_2(\cos\theta), \quad (24)$$

where

$$\begin{aligned} \xi_0 &= -\mathcal{P}_0(\epsilon + p) \left(\frac{dp}{dr} \right)^{-1}, \\ \xi_2 &= -\mathcal{P}_2(\epsilon + p) \left(\frac{dp}{dr} \right)^{-1}. \end{aligned} \quad (25)$$

Finally, we can calculate the radius of the pole R_{POL} and the radius of the equator R_{EQ} [1, 24]

$$R_{POL} = R + \xi_0 + \xi_2, \quad (26)$$

$$R_{EQ} = R + \xi_0 - \frac{\xi_2}{2}. \quad (27)$$

This allows us to calculate the eccentricity

$$e = \sqrt{1 - \frac{R_{POL}^2}{R_{EQ}^2}}. \quad (28)$$

Furthermore, in the original papers of HT formalism [19, 20], the maximum angular velocity of a rotating body within Newtonian gravity is mentioned, i.e.

$$\Omega_{max} = \sqrt{M_0/R^3}. \quad (29)$$

However, in the context of GR, the maximum angular velocity of NSs (which is called as Kepler frequency) is approximated by [24]

$$\Omega_K = 0.65 \sqrt{M_0/R^3}. \quad (30)$$

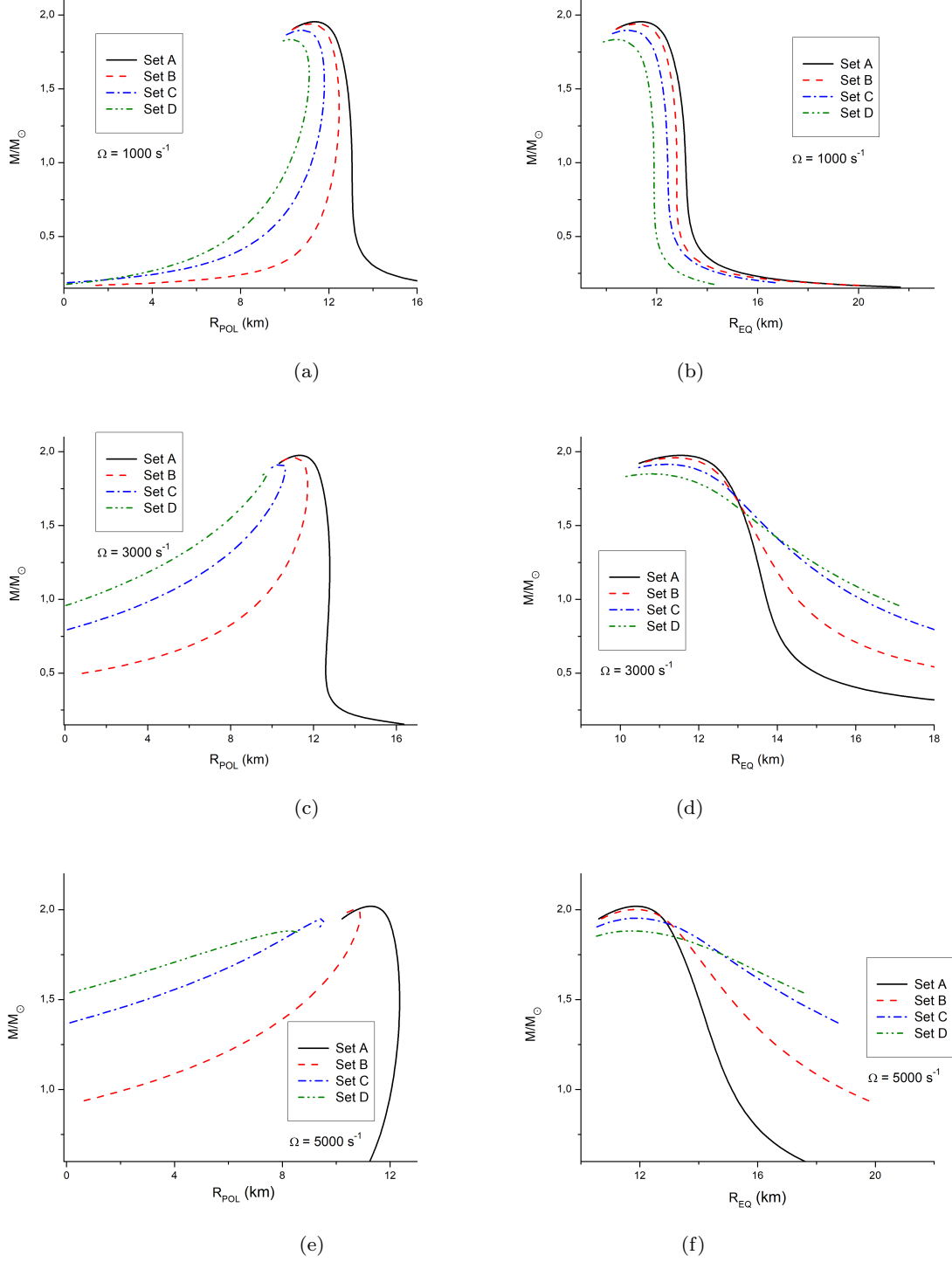


Fig. 2 Mass-radius relation of NSs for (a) polar radius at $\Omega = 1000 \text{ s}^{-1}$, (b) equatorial radius at $\Omega = 1000 \text{ s}^{-1}$, (c) polar radius at $\Omega = 3000 \text{ s}^{-1}$, (d) equatorial radius at $\Omega = 3000 \text{ s}^{-1}$, (e) polar radius at $\Omega = 5000 \text{ s}^{-1}$, and (f) equatorial radius at $\Omega = 5000 \text{ s}^{-1}$.

Table 1 Parameter sets of the magnetic fields

Set's name	B_0 (G)	B_{surf} (G)
Set A	0	0
Set B	1×10^{18}	1×10^9
Set C	2×10^{18}	1×10^{12}
Set D	3×10^{18}	1×10^{15}

Moreover, another important physical quantity to consider is the moment of inertia. With the angular momentum L and the angular velocity relative to the distant observers Ω in our hands, we can determine the moment of inertia

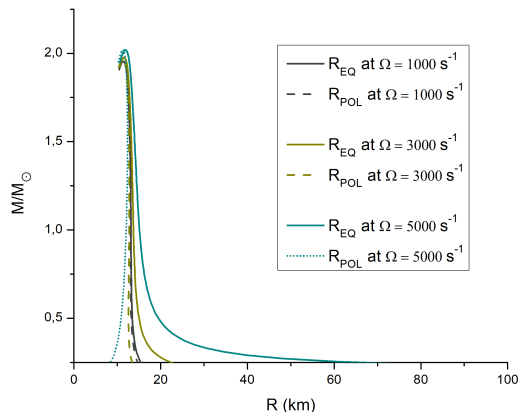
$$I = \frac{L}{\Omega}. \quad (31)$$

3 Results and Discussion

We numerically solved all differential equations using Euler method. For the value of Ω , we use $\Omega = 1000 \text{ s}^{-1}$, $\Omega = 3000 \text{ s}^{-1}$, and $\Omega = 5000 \text{ s}^{-1}$. For the initial value of $\bar{\omega}$ (i.e. ω_c), we choose 80 s^{-1} in this work. Please note that this value is much less than the value used in Ref. [37], i.e. $\bar{\omega} = 3000 \text{ s}^{-1}$. Moreover, it is also worth noting that $\bar{\omega}(r)$ increases with r , which would result in a large $\bar{\omega}$ value at the surface if a large initial ω_c is chosen. On the other side, we have insight that according to Ref. [38], the HT formalism is accurate to better than 1 per cent even for the fastest millisecond pulsars. However, putting $\bar{\omega}_c = 3000 \text{ s}^{-1}$ in the calculation is still potential to be dangerous, for the HT formalism is basically an approximation for slowly rotating relativistic stars. So our value of $\bar{\omega}_c$ is safer than the one in Ref. [37].

If we compare our initial value of $\bar{\omega}$ to the ones of Ref. [1] and Ref. [23] which chose $\bar{\omega}_c = 0$, our choice of $\bar{\omega}_c$ is more realistic for general rotating NS, since their choice seems to only agree the NSs with very slow rotation. The same value of ω_c and same reasoning of the choice have been highlighted by authors in Ref. [30]. It is worth mentioning that Refs. [23,24] impose a limit on the angular velocity Ω , setting its value to 5000 s^{-1} . In line with these previous studies, we adopt the same limitation and restrict Ω to 5000 s^{-1} in our analysis. Moreover, the parameter sets of the magnetic field employed in this study are presented in Table ??.

Fig. 1 presents the mass-radius relationship of NSs in a static configuration. This relation purely comes from TOV equation. From the relation, we can see that the presence of a chaotic magnetic field can reduce the radius of NSs, as indicated by the leftward shift of the curves with increasing magnetic field strength, suggesting that a chaotic magnetic field can contribute to

**Fig. 3** Mass-radius relation of the deformed NSs without magnetic field.

greater compactness of the stars. Compactness, defined as the mass-to-radius ratio, is directly influenced by this field. Notably, the radius reduction is pronounced in the case where $B_0 = 3 \times 10^{18} \text{ G}$ and $B_{surf} = 10^{15} \text{ G}$, indicating that the radius decrease is non-linear with respect to the increase in the chaotic magnetic field.

Furthermore, NSs formed with stronger chaotic magnetic fields exhibit a lower maximum mass compared to those formed with weaker chaotic magnetic fields. Our findings, however, differ from those presented by Lopes & Menezes [21], who reported that chaotic magnetic fields increase the radius of NSs and allow for the formation of NSs with a higher maximum mass when the chaotic magnetic field is stronger. This discrepancy may be attributed to the different EOS employed in their study. It is well known that different EOS could produce different result [39]. Additionally, it is interesting to note that as the magnetic field strength increases, the mass-radius curve begins to resemble that of quark stars. For more detailed discussions on quark stars, please refer to Refs. [40,41,42,43,44,45,46,47,48,49]. Moreover, it is noteworthy that the curve transformation resembling that of a quark star was also reported in the study conducted by da Silva et al. [25], for rapidly rotating polytropic compact stars, where the polytropic EOS constant was set to 3.25×10^{11} , and the polytropic index was set to 0.7463.

Fig. 2 shows the polar and equatorial radii, indicating the deformation of rotating NSs. The deformation is less pronounced for the NSs with higher masses but becomes more evident for lower masses. This can be seen in the mass-radius relations of magnetized rotating NSs, where the curves in R_{POL} panels and R_{EQ} panels diverge significantly at lower mass values. A comparison with Fig. 3 which depicts rotating NSs without a mag-

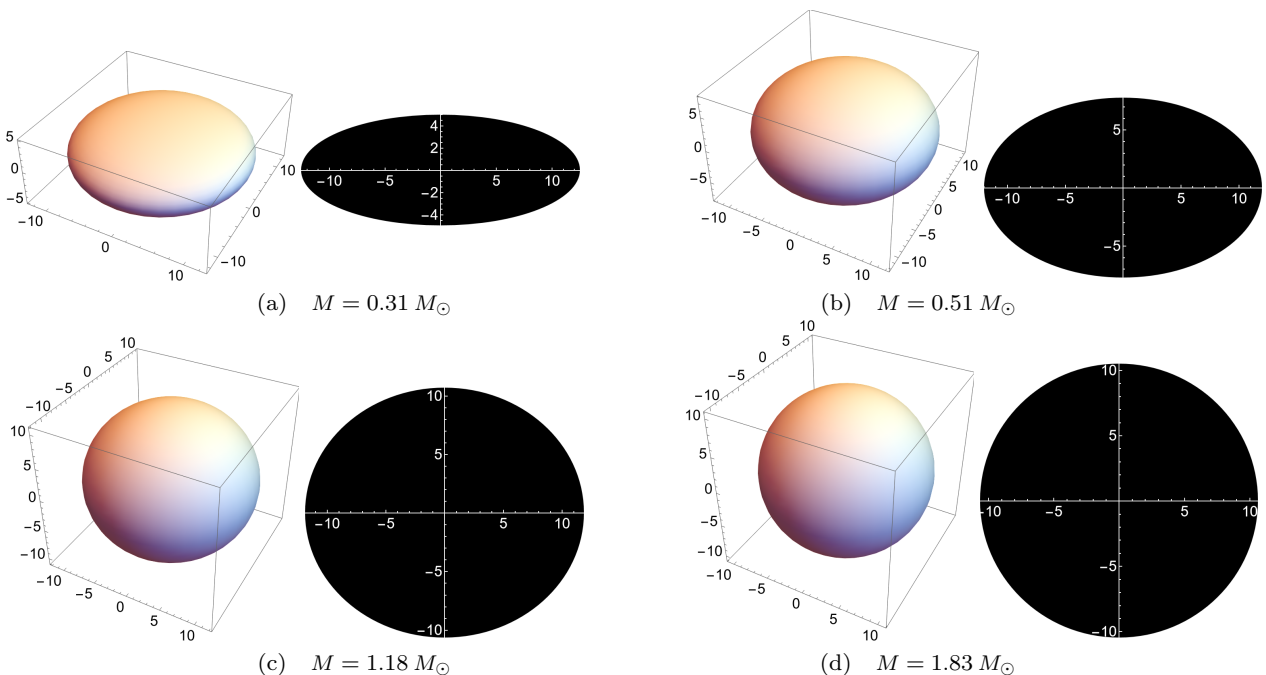


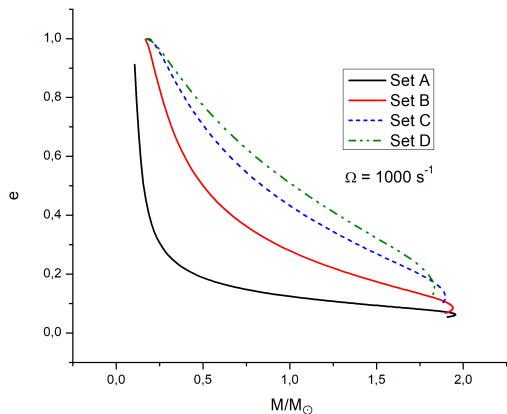
Fig. 4 Illustrations of 3- and 2-dimensional deformation of neutron stars in each particular mass at $B_0 = 3 \times 10^{18}$ G and $B_{surf} = 1 \times 10^{15}$ G at $\Omega = 1000$ s $^{-1}$.

netic field, reveals that deformation still occurs but with only slighter differences between the polar and equatorial radii. This deformation due to rotation is expected and is similar to the Earth’s rotational deformation, where the polar radius is smaller than the equatorial radius [1]. The key takeaway from Fig. 2 and Fig. 3 is that the deformation induced by the magnetic field is much more significant than that caused by rotation. It is worth noting that even though the magnetic field strengthens the deformation of the stars, the magnetic field in the static case shown by Fig. 1 does not cause the deformation, because the deformation in this context comes from quadrupole order of HT formalism. Since the magnetic field is embedded within the energy density and pressure which exist in the perturbative terms of HT formalism, so the magnetic field could impact on the deformation of the rotating NSs.

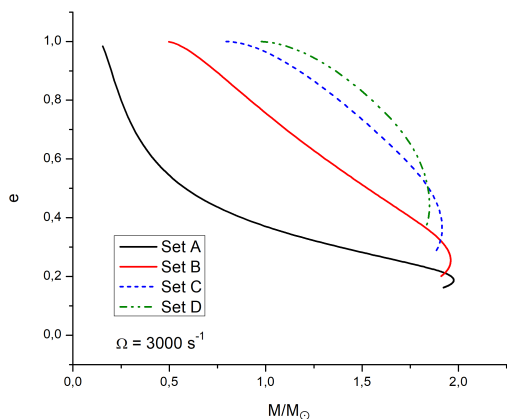
It is important to emphasize that the rotational aspect also plays an important role to deform the NSs. As shown in Fig. 2 and Fig. 3, higher values of Ω lead to a greater separation between the R_{POL} and R_{EQ} curves. Additionally, Fig. 2 demonstrates a substantial increase in deformation with increasing magnetic field strength. This contrasts with the findings in Ref. [11], where NSs were also deformed by the presence of a magnetic field, but the increase in deformation with increasing field strength was less pronounced, leading to nearly coincident curves. This difference may stem from differences in the ansatz and core EOS employed in their model.

We can also see that the magnetic field and the angular velocity relative to distant observers influence the minimum mass of the star. At $\Omega = 1000$ s $^{-1}$, all minimum mass values are below $0.25 M_\odot$. At $\Omega = 3000$ s $^{-1}$, the minimum mass for set A is significantly below $0.5 M_\odot$; the minimum mass for set B is approximately $0.5 M_\odot$; the minimum mass for set C is slightly above $0.75 M_\odot$; and the minimum mass for set D is slightly below $0.1 M_\odot$. At $\Omega = 5000$ s $^{-1}$, the minimum mass for set A is significantly below $0.5 M_\odot$; the minimum mass for set B is slightly below $1 M_\odot$; the minimum mass for set C is slightly above $1.25 M_\odot$; and the minimum mass for set D is slightly above $0.5 M_\odot$. From these results, we get an insight that although the chaotic magnetic field reduces the maximum mass, it conversely increases the minimum mass.

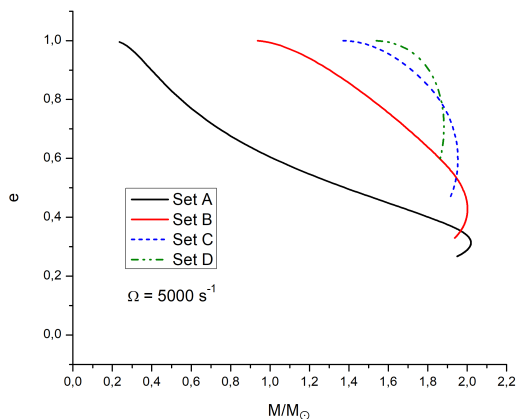
We present 3- and 2-dimensional illustrations of the NSs in Fig. 4. We take examples from the case of $B_0 = 3 \times 10^{18}$ G and $B_{surf} = 10^{15}$ G. At lower mass, the star’s shape becomes very oblate. At $M = 0.31 M_\odot$, $R_p = 4.96$ km, and $R_e = 12.51$ km; at $M = 0.51 M_\odot$, $R_p = 7.75$ km, and $R_e = 11.99$ km; $M = 1.18 M_\odot$, $R_p = 10.67$ km, and $R_e = 11.87$ km; and $M = 1.83 M_\odot$, $R_p = 10.48$ km, and $R_e = 10.63$ km. It is noteworthy to compare our results with those presented in Ref. [1]. The deformation of rotating NSs in our study is significantly more pronounced than in their findings, which are based on rotating NSs with anisotropic pressure of matter, but without considering the contribution of a



(a)



(b)



(c)

Fig. 5 Eccentricity of NSs at (a) $\Omega = 1000 \text{ s}^{-1}$, (b) $\Omega = 3000 \text{ s}^{-1}$, and (c) $\Omega = 5000 \text{ s}^{-1}$ as a function of mass.

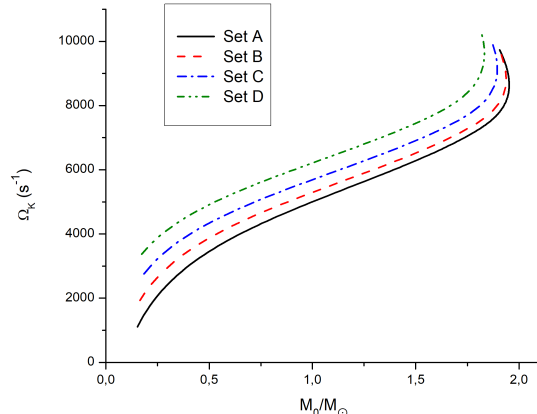


Fig. 6 Kepler frequency of NSs as a function of mass.

magnetic field to the deformation. This fact strengthens our argument that the magnetic field strongly induces the deformation of rotating NSs.

The oblateness of NSs can also be characterized by their eccentricity e . In the context of a two-dimensional body, when the value of e approaches 0, the shape of the body tends to be circular. Conversely, as e approaches 1, the shape becomes more elliptical. Fig. 5 illustrates the relationship between mass and eccentricity. Both rotation and chaotic magnetic fields contribute to an increased deformation of NSs, as higher values of Ω and B drive the eccentricity e closer to 1.

Furthermore, it is noteworthy to analyze the trends of the eccentricity curves. At $\Omega = 1000 \text{ s}^{-1}$, the trends of all curves are consistent with those reported in Ref. [24]. At $\Omega = 3000 \text{ s}^{-1}$, while the trends of sets A and B remain in agreement with Ref. [24], sets C and D exhibit a similarity to the trends seen in Ref. [1], where deformation arises from the combined effects of rotation and anisotropic pressure. Finally, at $\Omega = 5000 \text{ s}^{-1}$, the trend of set A continues to align with Ref. [24], whereas sets B, C, and D are consistent with the results presented in Ref. [1].

Fig. 6 illustrates the relationship between the M_0 and the Kepler frequency of NSs. The Kepler frequency increases with the strength of the chaotic magnetic field, indicating that NSs with stronger chaotic magnetic fields can rotate faster than those with weaker fields.

Previously, mass and radius calculations further reveal that rotating NSs with stronger chaotic magnetic fields exhibit lower maximum masses and smaller radii. This finding implies that for NSs rotating at their respective Kepler frequencies, our results align with angular momentum conservation. Specifically, stronger magnetic fields are associated with reduced maximum mass

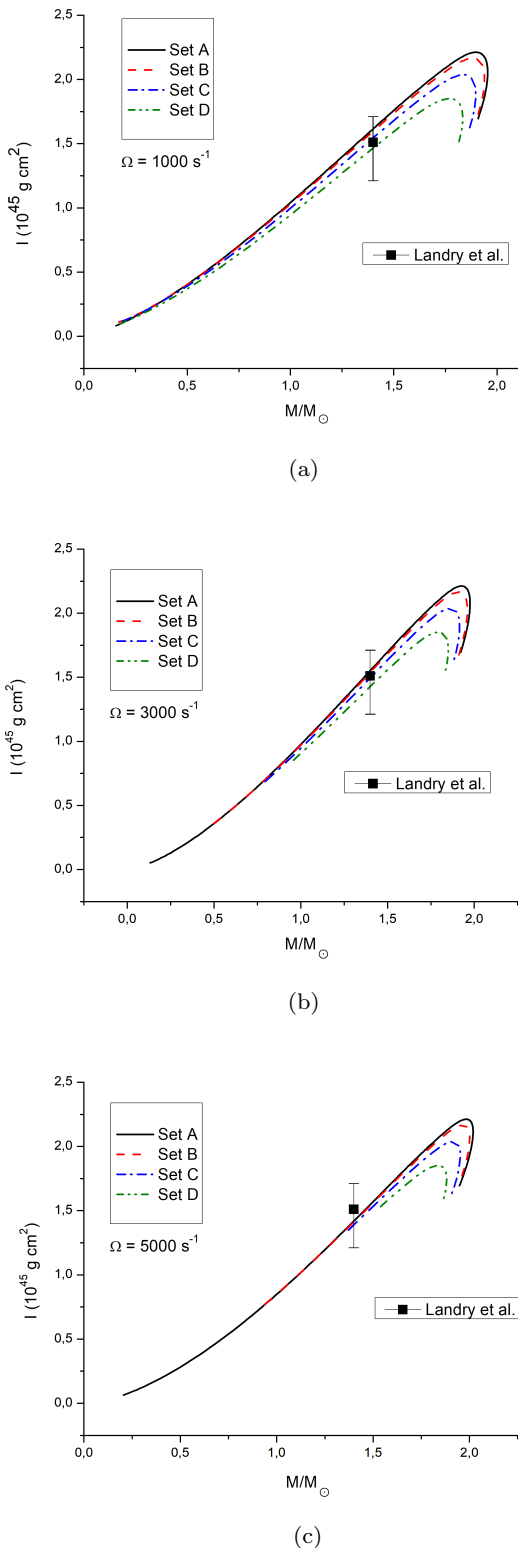


Fig. 7 Moment of inertia of NSs at (a) $\Omega = 1000 \text{ s}^{-1}$, (b) $\Omega = 3000 \text{ s}^{-1}$, and (c) $\Omega = 5000 \text{ s}^{-1}$ as a function of mass. Here we use a constraint range presented by Landry et al. [27].

and radius but an increased maximum angular velocity (i.e., Kepler frequency).

Fig. 7 depicts the relationship between the rotational mass and the moment of inertia of NSs. For $\Omega = 1000 \text{ s}^{-1}$, we can see that at lower masses, the curves tend to coincide, suggesting that the impact of chaotic magnetic field strength on the moment of inertia is negligible in this regime. However, a noticeable separation begins at $M = 0.5 M_{\odot}$, where stronger chaotic magnetic fields lead to a reduction in the moment of inertia. Given that the moment of inertia depends on both the mass and the square of the radius, these results are consistent with the mass-radius relations.

Remarkably, our findings for the moment of inertia at $\Omega = 1000 \text{ s}^{-1}$ and $\Omega = 3000 \text{ s}^{-1}$ are consistent with the constraint range provided by Landry et al. [27]. It is worth noting that this constraint evaluates whether rotating NSs with chaotic magnetic fields align with observational evidence. The constraint is given as $I = 1.51^{+0.20}_{-0.30} \times 10^{45} \text{ g cm}^2$ at $M = 1.4 M_{\odot}$, the standard mass of NSs. As detailed in Ref. [27], this constraint is derived from measurements of pulsar masses, gravitational wave signals from events such as GW170817 and GW190425, and X-ray data from hotspot emissions on NS surfaces observed by NICER. For the value of $M = 1.4 M_{\odot}$, it is noteworthy that observational data suggest NSs predominantly exist within a relatively narrow mass range close to $1.4 M_{\odot}$ [50].

4 Conclusion

In this study, we calculated the mass and radius of NSs under the influence of a chaotic magnetic field, enabling us to obtain the mass-radius relationship for these stars. Our findings indicate that the magnetic field can decrease the radius of NSs. NSs formed with stronger chaotic magnetic fields exhibit a lower maximum mass compared to those formed with weaker chaotic magnetic fields. Additionally, while the chaotic magnetic field can contribute to a reduction in radius, it can simultaneously enhance the compactness and deformation of rotating NSs. As the magnetic field strength increases, the mass-radius curve begins to resemble that of quark stars. For deformed rotating NSs, significant deformations occur at lower mass values.

On the other side, our results indicate that the presence of chaotic magnetic field enhances the Kepler frequency of rotating NSs, whereas it simultaneously tend to decrease their moment of inertia. Additionally, the moment of inertia of rotating NSs with chaotic magnetic fields at $\Omega = 1000 \text{ s}^{-1}$ and $\Omega = 3000 \text{ s}^{-1}$ is consistent with the constraint range obtained from pulsar mass measurements, gravitational wave event data

(GW170817 and GW190425), and X-ray observations of emissions from hotspots on NS surfaces measured by NICER.

Acknowledgements Special thanks are given to Anna Campoy Ordaz for making her code publicly available, which allowed MLP to modify it for use in this work. MLP acknowledges the Indonesia Endowment Fund for Education Agency (LPDP) for financial support. FPZ and GH would like to thank Kemendikisaintek (The Ministry of Higher Education, Science, and Technology) of the Republic of Indonesia (through LPPM ITB, Indonesia) for partially financial support. HLP and MLP would like to thank the members of the Theoretical Physics Groups at Institut Teknologi Bandung for their hospitality. MFARS is supported by the Second Century Fund (C2F), Chulalongkorn University, Thailand.

References

1. M.L. Pattersons, A. Sulaksono, *Eur. Phys. J. C* **81** 698 (2021).
2. I. Vidaña, *Eur. Phys. J. Plus* **133** 445 (2018).
3. A. Reisenegger, *ASP Conf. Ser.* **248** 469–478 (2001).
4. V. Graber, N. Andersson, M. Hogg, *Int. J. Mod. Phys. D* **26** 1730015 (2017). arXiv:1610.06882 [astro-ph.HE].
5. S. Ghosh, S. Shaikh, P.J. Kalita, P. Routaray, B. Kumar, B.K. Agrawal, *Nucl. Phys. B* **1008** 116697 (2024).
6. C. Sivaram, K. Arun, *Open Astron. J.* **5** 7–11 (2012).
7. J.M. Cohen, A. Rosenblum, *Astrophys. Space Sci.* **16** 130–136 (1972).
8. J.E. Horvath, *Int. J. Mod. Phys. D* **13** 1327–1334 (2004). arXiv:astro-ph/0404324.
9. A. Lyne, F. Graham-Smith, P. Weltevrede, C. Jordan, B. Stappers, C. Bassa, M. Kramer, *Science* **342** 598–601 (2013).
10. A. Basu, P. Char, R. Nandi, B.C. Joshi, D. Bandyopadhyay, *Astrophys. J.* **866** 2 (2018).
11. R. Rizaldy, A. Sulaksono, *J. Phys. Conf. Ser.* **1080** 012031 (2018).
12. B. Franzon, V. Dexheimer, S. Schramm, *Phys. Rev. D* **94** 044018 (2016).
13. M.L. Pattersons, F.P. Zen, arXiv:2411.11558 [gr-qc].
14. R. Rizaldy, A. Sulaksono, *J. Phys. Conf. Ser.* **1011** 012083 (2018).
15. G. Desvignes, P. Weltevrede, Y. Gao, et al., *Nature Astron.* **8** 617–627 (2024).
16. J.F. Fortin, H.K. Guo, K. Sinha, S.P. Harris, D. Kim, C. Sun, *Int. J. Mod. Phys. D* **30** 2130002 (2021). arXiv:2102.12503 [hep-ph].
17. K. Konno, T. Obata, Y. Kojima, *Astron. Astrophys.* **356** 234–237 (2000).
18. R. Mallick, S. Schramm, *Phys. Rev. C* **89** 045805 (2014).
19. J.B. Hartle, *Astrophys. J.* **150** 1005–1029 (1967).
20. J.B. Hartle, K.S. Thorne, *Astrophys. J.* **153** 807–834 (1968).
21. L. Lopes, D. Menezes, *J. Cosmol. Astropart. Phys.* **2015** 002 (2015). arXiv:1411.7209 [astro-ph.HE].
22. D.H. Wen, W. Chen, Y.G. Lu, L.G. Liu, *Chin. Phys. Lett.* **24** 628 (2007).
23. A.C. Ordaz, Master’s Thesis, Universitat de Barcelona, 2019.
24. L.L. Lopes, *Astrophys. J.* **966** 184 (2024).
25. F.M. da Silva, L.C.N. Santos, C.C. Barros Jr, *Class. Quantum Grav.* **38** 165011 (2021).
26. A. Rahmansyah, A. Sulaksono, A.B. Wahidin, A.M. Setiawan, *Eur. Phys. J. C* **80** 769 (2020).
27. P. Landry, R. Essick, K. Chatziioannou, *Phys. Rev. D* **101** 123007 (2020).
28. A. Sulaksono, *Int. J. Mod. Phys. E* **24** 1550007 (2015). arXiv:1412.7247 [nucl-th].
29. T. Miyatsu, S. Yamamuro, K. Nakazato, *Astrophys. J.* **777** 1 (2013).
30. M.L. Pattersons, F.P. Zen, H.L. Prihadi, M.F.A.R. Sakti, arXiv:2404.01837 [gr-qc].
31. S. Kumar, R. Bhattacharyya, B. Dasgupta, M.S. Janaki, *Phys. Plasmas* **24** 082902 (2017).
32. B. Dasgupta, A.K. Ram, G. Li, X. Li, *AIP Conf. Proc.* **1582** 213 (2014).
33. P. Beltracchi, C. Posada, *Phys. Rev. D* **110** 024052 (2024).
34. L.M. Becerra, E.A. Becerra-Vergara, F.D. Lora-Clavijo, *Phys. Rev. D* **110** 103004 (2024).
35. Y.B. Zel’dovich, I.D. Novikov, *Stars and Relativity* (Dover Publications, New York, 1971).
36. J.R. Oppenheimer, G.M. Volkoff, *Phys. Rev.* **55** 374 (1939).
37. D.H. Wen, W. Chen, L.G. Liu, *Chin. Phys. Lett.* **22** 1604 (2005).
38. E. Berti, F. White, A. Maniopoulou, M. Bruni, *Mon. Not. R. Astron. Soc.* **358** 923–938 (2005).
39. I.A. Rather, A.A. Usmani, S.K. Patra, *Nucl. Phys. A* **1010** 122189 (2021).
40. M.K. Mak, T. Harko, *Int. J. Mod. Phys. D* **13** (01) 149–156 (2004).
41. P. Jaikumar, *Eur. Phys. J. C* **49** 199–203 (2007).
42. X.Y. Lai, R.X. Xu, *Mon. Not. R. Astron. Soc.* **398** L31–L35 (2009).
43. R. Rizaldy, A. Sulaksono, *J. Phys. Conf. Ser.* **1321** 022016 (2019).
44. J.E. Horvath, P.H.R.S. Moraes, *Int. J. Mod. Phys. D* **30** (03) 2150016 (2021). arXiv:2012.00917 [astro-ph.HE].
45. P.C. Chu, Y. Zhou, Y.Y. Jiang, et al., *Eur. Phys. J. C* **81** 93 (2021).
46. A. Li, *EPJ Web Conf.* **260** 04001 (2022).
47. J.M. Mkenyeleye, M. Juma, J.M. Sunzu, *Int. J. Mod. Phys. D* **32** (11) 2350081 (2023).
48. A. Issifu, F.M. da Silva, D.P. Menezes, *Eur. Phys. J. C* **84** 463 (2024).
49. M. Ju, P. Chu, X. Wu, H. Liu, *Eur. Phys. J. C* **85** 40 (2025).
50. L. Kaper, A. van der Meer, M. van Kerkwijk, E. van den Heuvel, *The Messenger* **126** 27–31 (2006).